MATERIALS CHEMISTRY

FRONTIERS







RESEARCH ARTICLE

View Article Online
View Journal | View Issue



Cite this: *Mater. Chem. Front.,* 2019, **3**, 2388

Received 23rd July 2019, Accepted 9th September 2019

DOI: 10.1039/c9qm00476a

rsc.li/frontiers-materials

Water-compatible fluorescent [2]rotaxanes for Au³⁺ detection and bioimaging†

Sing-Ming Chan, Fung-Kit Tang, Chak-Shing Kwan, Ching-Yau Lam, Sam C. K. Haub and Ken Cham-Fai Leung *

In this study, the synthesis of [2]rotaxanes as fluorescent metal ion sensors has been demonstrated. [2]Rotaxanes, RA-H·PF₆, RRA and RRB, undergo photoelectron transfer resulting in fluorescence quenching. Before the diimine (dynamic covalent bond) reduction on the macrocyclic ring, the dynamic [2]rotaxane RA-H·PF₆ can be hydrolyzed and turned fluorescent by trivalent metal ions, giving fluorescence at λ_{max} 424 nm. After reduction of the imines, the reduced [2]rotaxanes RRA and RRB are kinetically stable and highly selective to Au³⁺ binding among 27 metal ions in a water-compatible (50 vol%) solution with working fluorescence in the range of pH 4–10. 50-Fold and 1.2-fold fluorescence turn-on after addition of Au³⁺ has been observed for RRA and RRB, respectively. Metal interference on Au³⁺ detection is insginificant, and thereby the fluorescence intensity is linearly proportional to the concentration of Au³⁺ until excess. The solid-state crystal structure of RRA shows the mechanically interlocked structure (mechanical bond). The bioimaging experiment of RRB with HeLa cells demonstrates the potential application of these mechanically interlocked molecules for metal ion detection in aqueous media and biological systems.

Introduction

Simple organic molecules have been used as fluorescent metal ion sensors due to their high selectivity, sensitivity, simplicity, quick response and feasibility of both in vitro and in vivo testing. 1-4 In particular, rotaxanes, mechanically interlocked molecules with unique topology,^{5,6} have been in the spotlight for ion sensing over the past few decades. Compared to conventional sensors, the interlocked system of rotaxanes can provide a dynamic and yet switchable cavity, thus allowing them to bind specific analytes selectively.⁷ The mechanical bond can also provide unusual coordination geometries and augmented redox activity as a potential ligand.8 It was first reported by Hiratani and co-workers as a selective Li⁺ fluorescent rotaxane sensor in CH₂Cl₂/MeCN solution (90:10, v/v).⁹ Previously, Goldup and co-workers reported a [2]rotaxane fluorescent sensor for Zn²⁺ in MeCN/H₂O solution (98:2, v/v).¹⁰ In another study performed by Beer and co-workers, they designed a rotaxane for sensing halide ions in up to 35% H₂O in MeCN.¹¹ Lin and co-workers also reported a [2]rotaxane for Fe³⁺ detection and bioimaging.¹² However, most of the rotaxane sensors focus on alkali metal ions,^{9,13,14} divalent transition metal ions^{10,15} and anions.^{11,16–18} In the case of precious metals and other platinum group elements (Pt, Pd, Rh, Ir, Ru, and Os), the application of using rotaxanes as a metal ion sensor in aqueous media is relatively unexplored, and thereby the effect of other metal ions as interference is seldom mentioned.¹⁰ Since the detection of metal ions in aqueous media has become crucial in biological systems, the development of water-soluble rotaxane metal ion sensors has become highly desired.

Gold, one of the precious metals, has been utilized in functional nanoparticles. ¹⁹ In particular, its ion form, Au^{3+} , has been applied in biological, ^{20,21} catalysis, ^{22,23} and other industrial applications. ²⁴ For instance, recent studies have shown that an Au(III) complex could be used as an effective anticancer drug due to its tumor growth inhibiting properties. ²¹ Despite the advantages, excess Au^{3+} can damage the organs. ²⁵ For example, Au^{3+} can lead to inhibition of the oxygen consumption of liver and kidney slices. ²⁶ An Au^{3+} salt solution is over 90% toxic at a concentration of 200 μ M. ²⁷ Thus, the detection of Au^{3+} has become crucial.

Herein, we report fluorescent [2]rotaxanes as selective metal ion sensors for detecting Au³⁺ and other trivalent metal ions in aqueous media by applying dynamic clipping on R₂NH₂⁺ for [2]rotaxane synthesis. It is part of dynamic covalent chemistry (DCC), which allows self-error checking and self-sorting to give the most thermodynamically stable rotaxane as the major product.²⁸⁻³⁶

^a Department of Chemistry, Hong Kong Baptist University, Kowloon Tong, Kowloon, Hong Kong SAR, P. R. China. E-mail: cfleung@hkbu.edu.hk

b Department of Chemistry, The Chinese University of Hong Kong, Shatin, New Territories, Hong Kong SAR, P. R. China

 $[\]dagger$ Electronic supplementary information (ESI) available. CCDC 1942423. For ESI and crystallographic data in CIF or other electronic format see DOI: 10.1039/c9qm00476a

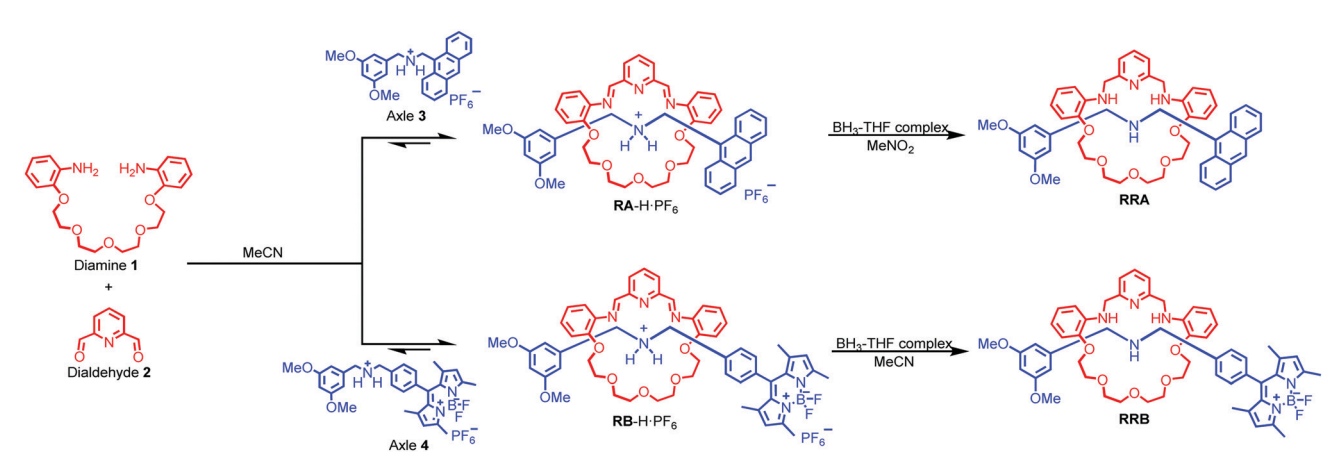
The rotaxanes reported in this project were obtained in high yield, having pyridine/amine nitrogen and ethylene glycol oxygen donor atom moieties for selective metal ion binding. First, the fluorescent response of the as-synthesized RA-H-PF6 and RB-H-PF6 with the trivalent metal ions in 1% H2O in MeCN was investigated. To increase the selectivity, RA-H-PF6 and RB-H-PF6 were further reduced, and the fluorescence response shows much significant improvement for RRA and RRB on detection of Au3+ ions in MeCN/H2O solution. In view of potential bio-application of rotaxanes such as drug delivery, 37-40 the cell viability of HeLa cells was performed to demonstrate the in vitro imaging of Au3+ with both RRA and RRB.

Results and discussion

As shown in Scheme 1, two dynamic rotaxanes, RA-H-PF₆ and RB-H-PF₆, were first synthesized for trivalent metal ion sensing. RA-H-PF₆ was thermodynamically formed via a clipping strategy with equal molar concentrations of tetraethylene glycol

bis(2-aminophenyl)ether (diamine 1), 2,6-pyridine dicarboxaldehyde (dialdehyde 2) and anthracene-based axle 3.41 On the other hand, RB-H·PF₆ was synthesized with 1, 2, and BODIPY-based axle 4 by using the same clipping strategy. After the [2]rotaxane formation, the original fluorescence from the anthracene-based and BODIPY-based axles could be quenched, which may be caused by the electron transfer from the imine and pyridine moieties within the macrocyclic ring. The fluorescence could be restored when the imine moieties of RA-H-PF6 hydrolyze back to the aldehyde and amine groups in the presence of acid or water, which leads to the dissociation of the macrocycle and separate components. The breakdown will then inhibit the internal electron transfer and provide a fluorescence band with λ_{max} at 424 nm.

The fluorescence response of RA-H-PF₆ towards cations Li⁺, $\begin{array}{l} NH_4^{\ +}, Na^+, K^+, Ag^+, Cs^+, Mg^{2^+}, Ca^{2^+}, Mn^{2^+}, Fe^{2^+}, Co^{2^+}, Ni^{2^+}, Cu^{2^+}, \\ Zn^{2^+}, \ Pd^{2^+}, \ Cd^{2^+}, \ Pt^{2^+}, \ Hg^{2^+}, \ Pb^{2^+}, \ Al^{3^+}, \ V^{3^+}, \ Cr^{3^+}, \ Fe^{3^+}, \ Ru^{3^+}, \end{array}$ Rh³⁺, Ce³⁺, Ir³⁺ and Au³⁺ was first investigated in a MeCN/H₂O (99:1, v/v) co-solvent system. As shown in Fig. 1, the fluorescence of RA-H-PF₆ was turned on significantly by 5 equivalents



Scheme 1 Synthesis of [2] rotaxanes with anthracene and BODIPY as a stopper and fluorophore.

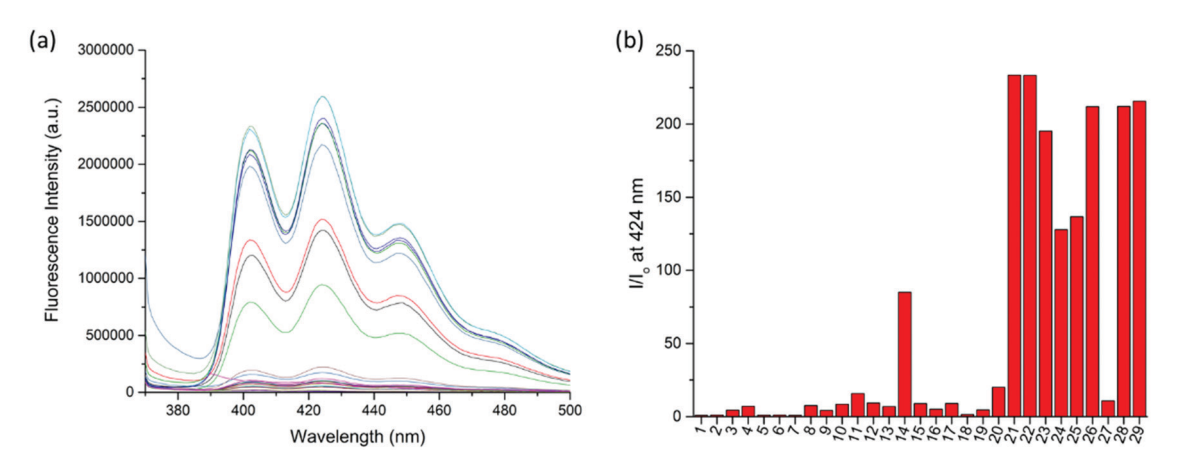


Fig. 1 (a) Fluorescence spectra of RA-H-PF₆ (20 μ M, λ_{ex} = 360 nm) upon addition of 5 equiv. of M^{n+} in MeCN/H₂O solution (99 : 1, v/v). (b) Fluorescence response of **RA**-H-PF₆ (20 μ M, λ_{ex} = 360 nm) to 5 equiv. of Mⁿ⁺ at 424 nm. (1) Blank, (2) Li⁺, (3) NH₄⁺, (4) Na⁺, (5) K⁺, (6) Ag⁺, (7) Cs⁺, (8) Mg²⁺, (9) Ca²⁺, (10) Mn²⁺, (11) Fe²⁺, (12) Co²⁺, (13) Ni²⁺, (14) Cu²⁺, (15) Zn²⁺, (16) Pd²⁺, (17) Cd²⁺, (18) Pt²⁺, (19) Hg²⁺, (20) Pb²⁺, (21) Al³⁺, (22) V³⁺, (23) Cr³⁺, (24) Fe³⁺, (25) Ru³⁺, (26) Rh³⁺, (27) Ce³⁺, (28) Ir³⁺ and (29) Au³⁺

Scheme 2 Plausible mechanism of switch on fluorescence of RA-H-PF₆ to trivalent metal ions via rotaxane dissociation.

of common trivalent metal ions like Al³⁺, V³⁺, Cr³⁺, Fe³⁺, Ru³⁺, Rh³⁺, Ir³⁺ and Au³⁺, along with moderate fluorescence turn-on by a divalent metal ion (Cu²⁺). These results indicate that dynamic [2]rotaxane RA-H·PF₆ is relatively selective to reported trivalent metal ion binding. Al, V, Cr, and Fe are high abundance elements on Earth. Ru, Rh, Ir and Au are commonly used as catalysts for organic reactions. Since those trivalent metal ions are Lewis acids, they could induce acid hydrolysis of the imine moiety of RA-H·PF₆ upon binding to the dynamic [2]rotaxane (Scheme 2). To study the mechanism, NMR spectroscopic titration experiments were conducted. The stacked ¹H NMR spectra (Fig. 2) illustrate that the addition of trivalent metal ions could decrease the amount of imine protons of RA-H-PF₆ while increasing the amount of aldehyde protons. This also supports that the hydrolyzed RA-H·PF₆ could be separated into diamine, dialdehyde and axle components upon the addition of trivalent metal ions. Moreover, the axle 3 could restore its fluorescence because of the absence of PET.

With the aim to investigate another metal sensing mechanism without cleavage of the macrocyclic ring of dynamic [2]rotaxane, the imine moieties on the macrocycle of the dynamic [2]rotaxane RA-H·PF₆ and RB-H·PF₆ were then reduced by BH₃-THF complex (Scheme 1), yielding diamine-based, kinetically stable [2]rotaxanes RRA and RRB. After the purification by column chromatography, RRA and RRB were obtained in 70% and 75% yield, respectively. The X-ray crystallography analysis of RRA single crystal shows the existence of the interlocking structure (mechanical bond) in the solid-state structure (Fig. 3), confirming successful diimine reduction to form the RRA.

The selectivity of the reduced rotaxanes to cations was investigated. Since the solubility of RRA is relatively low at

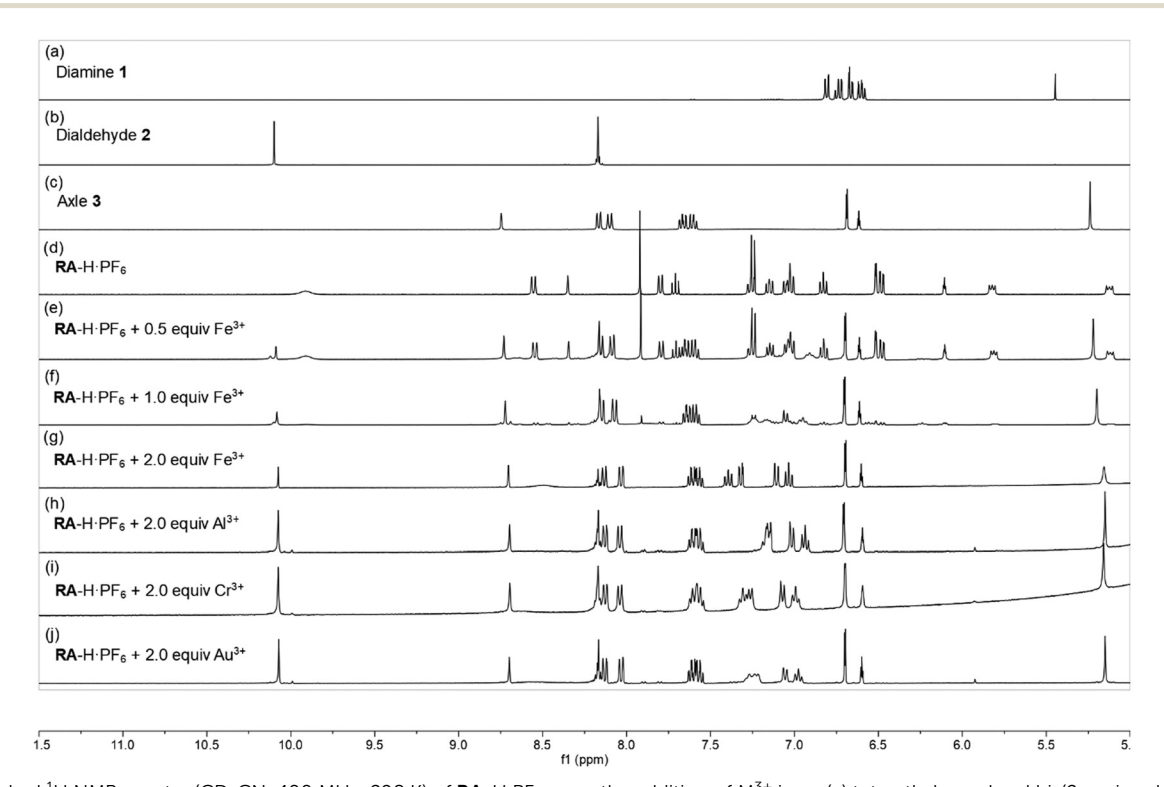


Fig. 2 Stacked ¹H NMR spectra (CD₃CN, 400 MHz, 298 K) of **RA**-H-PF₆ upon the addition of M³⁺ ions: (a) tetraethylene glycol bis(2-aminophenyl)ether, (b) 2,6-pyridine dicarboxaldehyde, (c) anthracene axles 1, (d) RA-H·PF₆, (e) RA-H·PF₆ + 0.5 equiv. of Fe³⁺, (f) RA-H·PF₆ + 1.0 equiv. of Fe³⁺, (g) RA-H·PF₆ 2.0 equiv. of Fe³⁺, (h) **RA**-H-PF₆ + 2.0 equiv. of Al³⁺, (i) **RA**-H-PF₆ + 2.0 equiv. of Cr³⁺ and (j) **RA**-H-PF₆ + 2.0 equiv. of Au³⁺

Research Article

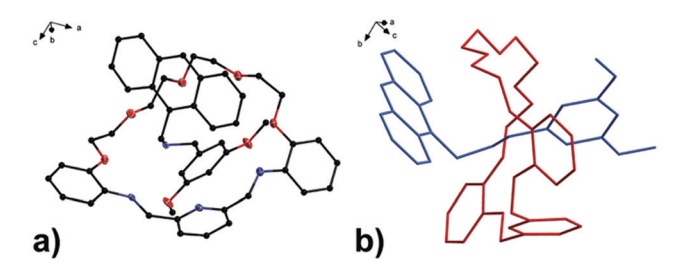


Fig. 3 (a) Perspective view of solid-state structures of reduced [2]rotaxane RRA; (b) discriminative view of solid-state structures of reduced [2]rotaxane RRA. CCDC code: 1942423.†

MeCN, THF was used to dissolve RRA. After the diimine reduction, the fluorescence response of RRA in THF/MeCN/ H₂O solution (2:48:50, v/v/v) had more than 50-fold enhancement on fluorescence intensity at 417 nm with 10.0 equiv. of Au³⁺. The fluorescence response has significantly improved and can only be turned on by Au³⁺ (Fig. 4). This suggests that Au³⁺ could inhibit the PET of RRA. In comparison with RRA, the

response of RRB has 1.2-fold enhancement upon the addition of 10.0 equiv. of Au3+ and 0.6-fold enhancement upon the addition of 10.0 equiv. of Hg2+ and Cu2+ separately in MeCN/ H_2O solution (50:50, v/v). Next, the metal interference on Au^{3+} detection was tested. To study the interference, RRA and RRB were added to a mixture of Au³⁺ and one of the metal ions used in the previous experiment. The fluorescence response of rotaxanes to Au³⁺ is similar in the presence of most of the metal ions except for Pd2+, Ru3+ and V3+, suggesting that the interference from other metal ions was insignificant (Fig. 4b). The quenching of Pd2+, Ru3+ and V3+ may be due to the similar size with Au³⁺, having an effective ionic radius of 86, 68, 64 and 85 pm respectively.

Since both **RRA** and **RRB** show high selectivity to Au³⁺, NMR titration of Au³⁺ was performed and illustrated (Fig. 5). Upon addition of Au³⁺, the ¹H NMR spectra of RRA and RRB changed dramatically, exhibiting a similar pattern to the acid-equilibrium form of both RRA and RRB. Moreover, the appearance of ammonium protons (H_c) also proved that the dialkylamine of RRA (H_c δ 8.89 ppm) and **RRB** (H_c δ 8.99 ppm) was protonated by Au³⁺.

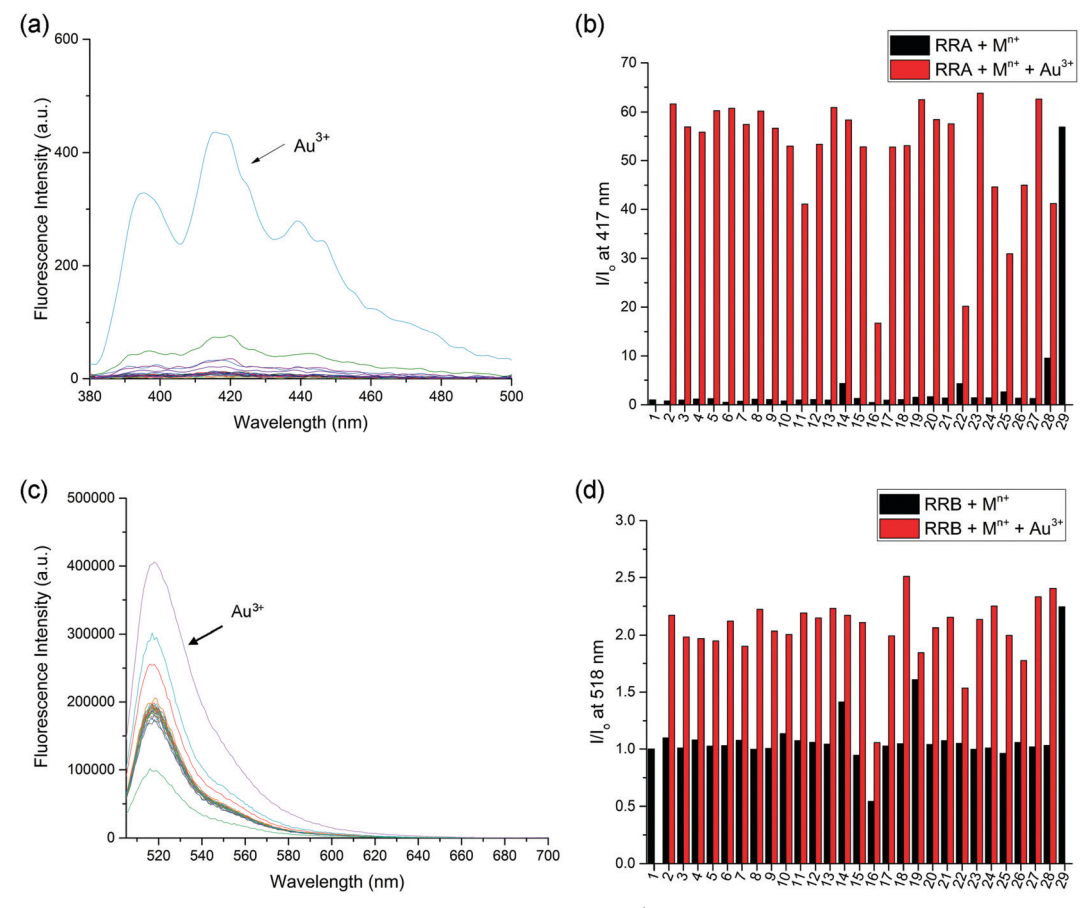
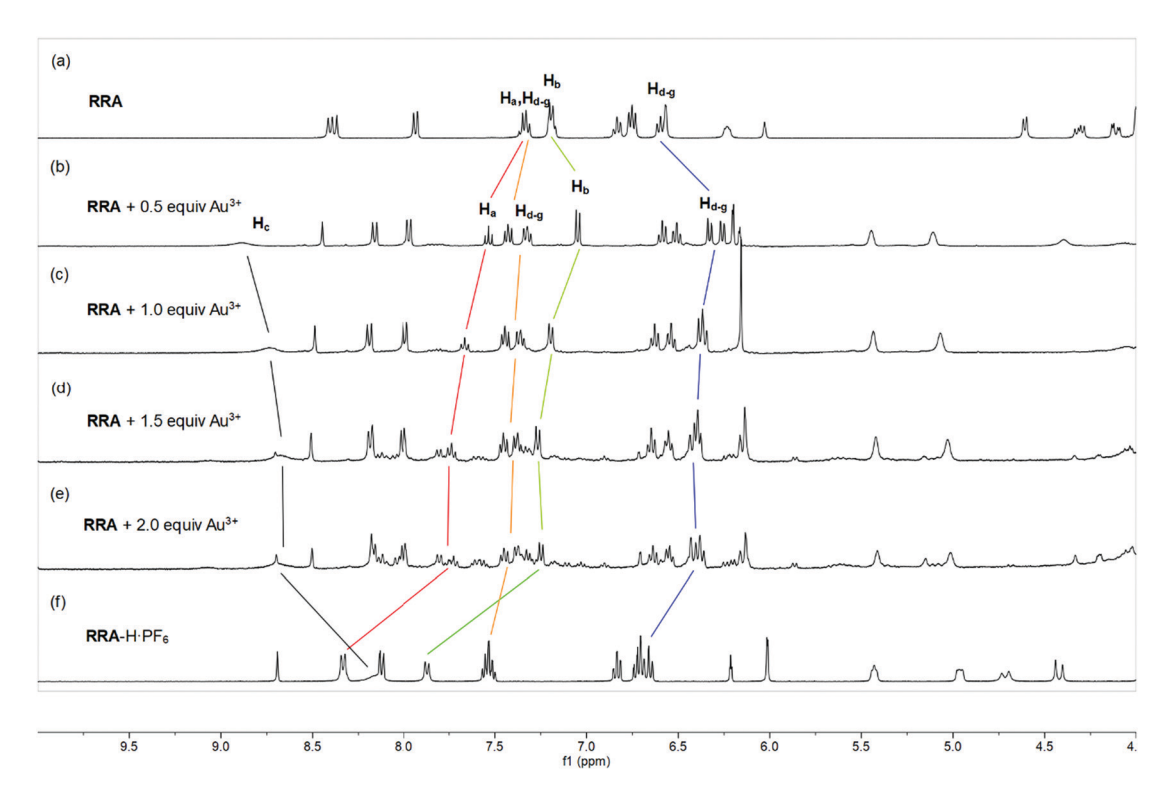


Fig. 4 (a) Fluorescence spectra of RRA (20 μ M, λ_{ex} = 370 nm) with 10 equiv. of Mⁿ⁺ in THF/MeCN/H₂O solution (2:48:50, v/v/v). (b) Fluorescence response of RRA (20 μ M, λ_{ex} = 370 nm) to 10 equiv. of M^{n+} at 417 nm indicated by black bars; RRA and different metal ion solutions upon addition of 10 equiv. of Au^{3+} indicated by red bars. (c) Fluorescence spectra of **RRB** (5 μ M, λ_{ex} = 500 nm) with 10 equiv. of M^{n+} in MeCN/H₂O solution (50 : 50, v/v). (d) Fluorescence response of **RRB** (5 μ M, λ_{ex} = 500 nm) to 10 equiv. of Mⁿ⁺ at 518 nm indicated by black bars; **RRA** and different metal ion solutions upon addition of 10 equiv. of Au^{3+} indicated by red bars. (1) Blank, (2) Li^+ , (3) NH_4^+ , (4) Na^+ , (5) K^+ , (6) Ag^+ , (7) Cs^+ , (8) Mg^{2+} , (9) Ca^{2+} , (10) Mn^{2+} , (11) Fe^{2+} , (12) Co^{2+} , (13) Ni^{2+} , (14) Cu^{2+} , (15) Zn^{2+} , (16) Pd^{2+} , (17) Cd^{2+} , (18) Pt^{2+} , (19) Hg^{2+} , (20) Pb^{2+} , (21) Al^{3+} , (22) V^{3+} , (23) Cr^{3+} , (24) Fe^{3+} , (25) Ru^{3+} , (26) Rh^{3+} , (27) Ce^{3+} , (27) Ce^{3+} , (28) Rl^{3+} , (29) Rl^{3+} , (29) Rl^{3+} , (29) Rl^{3+} , (21) Rl^{3+} , (22) Rl^{3+} , (23) Rl^{3+} , (24) Rl^{3+} , (25) Rl^{3+} , (26) Rl^{3+} , (27) Rl^{3+} , (27) Rl^{3+} , (28) Rl^{3+} , (29) Rl^{3+} , (29) Rl^{3+} , (29) Rl^{3+} , (21) Rl^{3+} , (21) Rl^{3+} , (22) Rl^{3+} , (23) Rl^{3+} , (24) Rl^{3+} , (25) Rl^{3+} , (26) Rl^{3+} , (27) Rl^{3+} , (28) Rl^{3+} , (29) Rl^{3+} , (21) Rl^{3+} , (22) Rl^{3+} , (23) Rl^{3+} , (24) Rl^{3+} , (25) Rl^{3+} , (26) Rl^{3+} , (27) Rl^{3+} , (28) Rl^{3+} , (29) Rl^{3+} , (21) Rl^{3+} , (21) Rl^{3+} , (22) Rl^{3+} , (23) Rl^{3+} , (24) Rl^{3+} , (25) Rl^{3+} , (26) Rl^{3+} , (27) Rl^{3+} , (28) Rl^{3+} , (29) Rl^{3+} , (21) Rl^{3+} , (22) Rl^{3+} , (23) Rl^{3+} , (24) Rl^{3+} , (25) Rl^{3+} , (27) Rl^{3+} , (28) Rl^{3+} , (28) Rl^{3+} , (29) Rl^{3+} , (2 (28) Ir^{3+} and (29) Au^{3+}



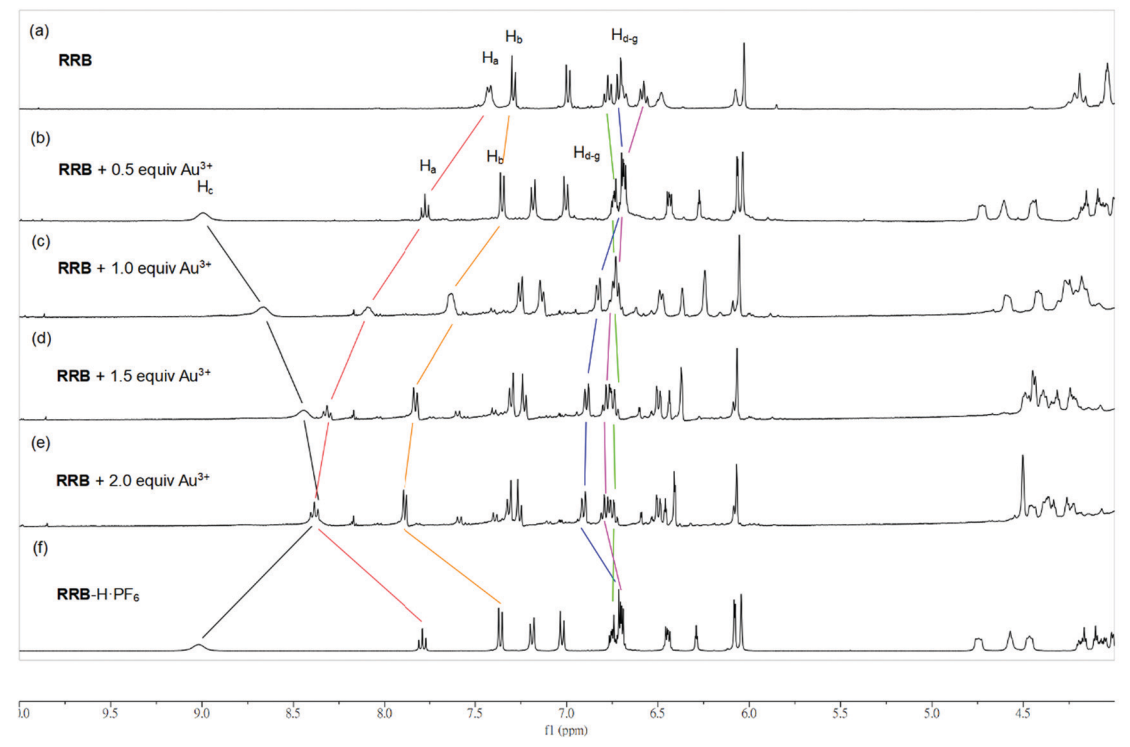


Fig. 5 Stacked ¹H NMR spectra (CD₃CN, 400 MHz, 298 K) of RRA (upper) and RRB (lower) upon addition of (a) 0, (b) 0.5, (c) 1.0 (d) 1.5, and (e) 2.0 equiv. of Au³⁺. (f) **RRA**-H·PF₆, and **RRB**-H·PF₆.

During the titration, chemical shifts of the pyridyl (Ha,b), ammonium proton (H_c) and phenyl (H_{d-g}) units which belong to the macrocyclic ring were observed, indicating their participation in the Au³⁺ complexation. Since the proton signal of both the axle and macrocycle has shifted during the complexation, we proposed that the Au³⁺ was bound inside the cavity of the rotaxanes (Scheme 3).

Research Article

Scheme 3 Plausible mechanism of switch on fluorescence of RRA and RRB upon addition of Au³⁺.

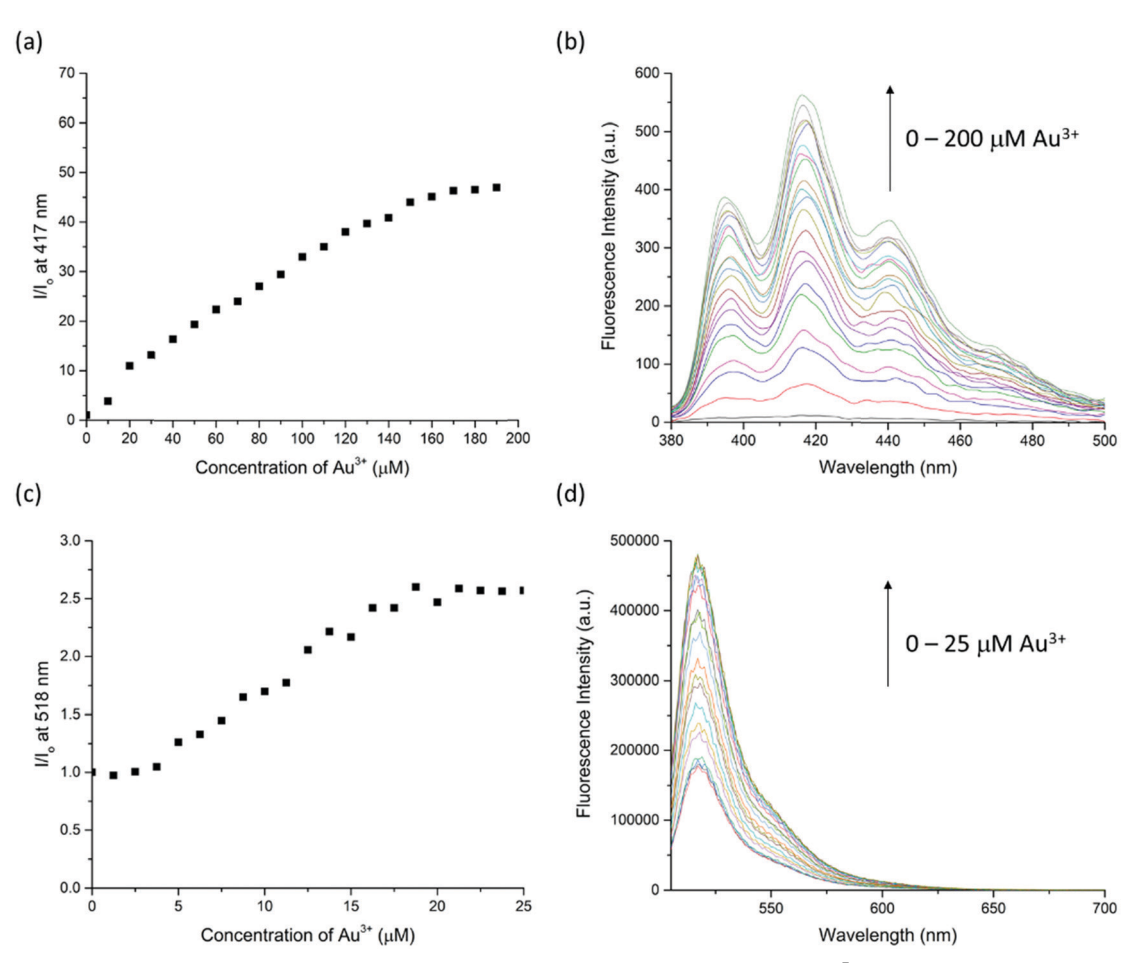


Fig. 6 (a) Fluorescence response of RRA (20 μ M, λ_{ex} = 370 nm) at 417 nm upon the addition of Au³⁺ (0-200 μ M) in THF/MeCN/H₂O solution (2:48:50, v/v/v). (b) Fluorescence spectral change of **RRA** (20 μM , λ_{ex} = 370 nm) at 417 nm upon addition of Au³⁺ (0-200 μM) in THF/MeCN/H₂O solution (2:48:50, v/v/v). (c) Fluorescence response of RRB (5 μ M, λ_{ex} = 500 nm) at 518 nm upon the addition of Au³⁺ (0-25 μ M) in MeCN/H₂O solution (50 : 50, v/v). (d) Fluorescence spectral change of **RRB** (5 μ M, λ_{ex} = 500 nm) at 518 nm upon addition of Au³⁺ (0–25 μ M) in MeCN/H₂O solution (50:50, v/v).

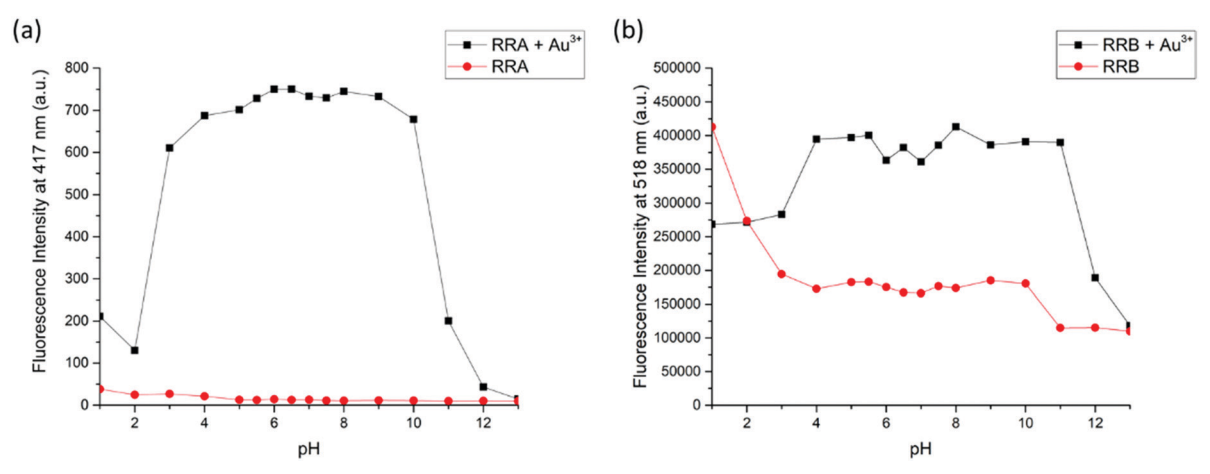


Fig. 7 (a) Fluorescence response of RRA (20 μ M, λ_{ex} = 370 nm) at 417 nm upon addition of 10 equiv. of Au³⁺ in THF/MeCN/H₂O solution (2:48:50, v/v/v) (pH 1-13) indicated by the black line; fluorescence of RRA at 417 nm in THF/MeCN/H₂O solution (2:48:50, v/v/v) (pH 1-13) indicated by the red line. (b) Fluorescence response of **RRB** (5 μ M, λ_{ex} = 500 nm) at 518 nm upon addition of 10 equiv. of Au³⁺ in MeCN/H₂O solution (50 : 50, v/v) (pH 1–13) indicated by the black line; fluorescence of RRB at 518 nm in MeCN/H₂O solution (50:50, v/v) (pH 1-13) indicated by the red line.

The sensitivity of Au3+ detection was studied by a fluorescence titration experiment (Fig. 6). Upon titration, the fluorescence intensity of RRA and RRB is linearly proportional to the increase of Au3+ concentration in the range of 0-160 µM and 5-20 µM, respectively. The intensity remains steady after the addition of 160 μM of Au^{3^+} to $\mbox{\it RRA}$ solution and 20 μM of Au³⁺ to **RRB**. The results indicate that the amount of Au³⁺ can be estimated by both rotaxane sensors. Indeed, the binding constant (K_a) with **RRA** to Au³⁺ is 9.05×10^3 M⁻¹ and that of

RRB with Au^{3+} is $2.92 \times 10^4 M^{-1}$, calculated by using the equation $K_a = B^{-1} \times [I_{\text{max}} - I_{\text{min}}]^{-1}$ from Benesi-Hildebrand analysis (Fig. S2 and S3, ESI†). This reveals that RRB can bind stronger to Au³⁺ than RRA.

Furthermore, because the NMR titration indicates that RRA and RRB were acidified during the binding to Au³⁺, the fluorescence response of RRA and RRB to Au3+ can be changed according to the pH equilibrium between the rotaxanes and their protonated form. Therefore, the fluorescence responses of

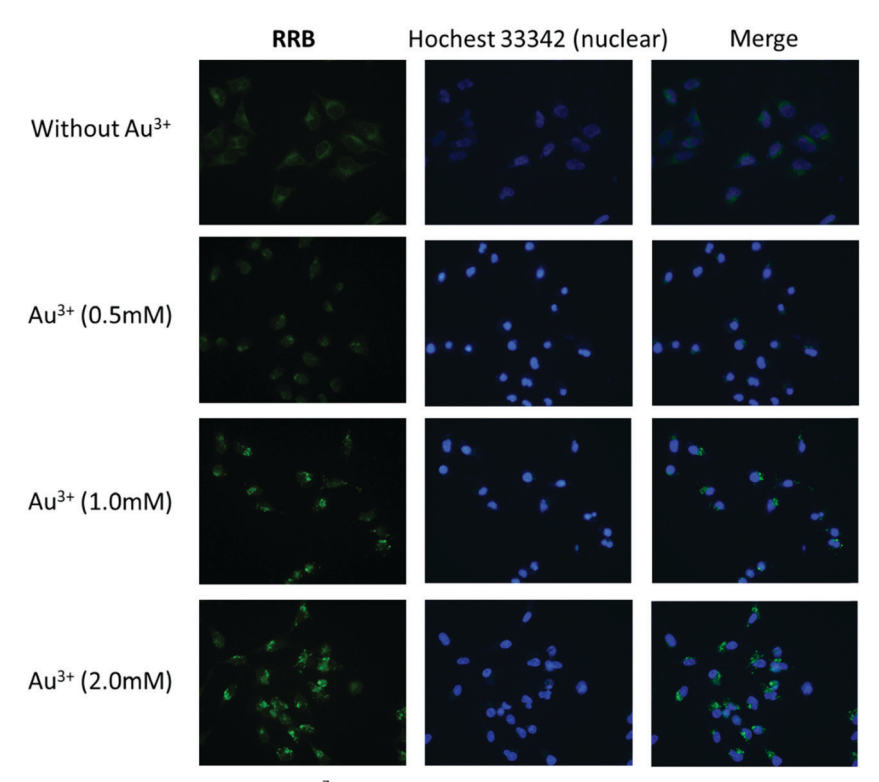


Fig. 8 Fluorescence images of HeLa cells pretreated with Au³⁺ (0, 0.5, 1.0 and 2.0 mM) for 24 h and then incubated with RRB for 2 h. The cell nuclei were stained with Hoechst 33342 (blue) (scale bar: 50 μm).

RRA and RRB were tested at different pH values (Fig. 7). Without Au³⁺, **RRA** has weak fluorescence in the pH range of 1.0-13.0. While the fluorescence of RRA was turned on significantly from pH 4.0-10.0 upon addition of Au³⁺. The results show that the Au³⁺ detection is partially pH independent with RRA when the pH is in the range of 4.0-10.0. For RRB, it gives weak fluorescence in the pH range of 3.0-13.0 without Au³⁺. Upon addition of Au³⁺, fluorescence was turned on significantly from pH 4.0-11.0. Under extreme acidic conditions, the pyridyl and amine units were protonated, which affects the binding to Au³⁺. Moreover, BODIPY was unstable and could not give reliable sensing results based on fluorescence signals at extremely acidic conditions (pH < 2).42 Under extreme alkali conditions, the environment facilitates the formation of gold hydroxide, which has a low water solubility $(K_{\rm sp} = 5 \times 10^{-46})$. Without dissolving gold ions in the solution, the formation of a sensor-metal complex is slow, so the fluorescence response of the rotaxanes is greatly reduced.

In addition to the titration experiment, the response time experiment was also conducted to investigate the sensitivity of **RRA** and **RRB** to Au^{3+} (Fig. S4, ESI†). The results show that the fluorescence intensity became steady around 15 min and 5 min for **RRA** and **RRB** respectively, suggesting that both sensors can be used for quick recognition. Moreover, the limit of detection (LOD) of **RRA** for Au^{3+} is 3.23 μM and **RRB** for Au^{3+} is 0.35 μM according to equation: LOD = $3\sigma/m$.

The cell viability of HeLa cells treated with **RRA** and **RRB** for 24 h was assessed using CCK-8 (Fig. S5, ESI†). As a result, the two sensors presented different toxic effects on HeLa cells. For **RRA** treated cells, the viability showed a remarkable decline at 0.2 μ M, while the viability in **RRB** treated cells only displayed a slight suppression at 2.0 μ M.

Since **RRA** was toxic to the cells even at low concentration (0.2 μ M), we only examined the ion detection ability using **RRB** in HeLa cells. It was found that **RRB** could stain the cells and show weak green fluorescence without Au³⁺ treatment (Fig. 8). After the pre-treatment of Au³⁺, the green fluorescence in the cells was obviously enhanced along with the increase of Au³⁺ concentration. Interestingly, the green fluorescence was mostly found in the vacuole-like organelles appearing as green light spots under a fluorescent microscope. This result suggests that **RRB** could detect Au³⁺ and present an ion concentration-dependent sensing capacity in HeLa cells.

Conclusion

In conclusion, we have synthesized new fluorescent [2]rotaxane sensors. The fluorescence properties of rotaxanes in metal ion detection have been demonstrated. Dynamic rotaxane RA-H·PF₆ can be hydrolyzed and its fluorescence switched on by common trivalent metal ions. For the reduced form of dynamic rotaxanes, RRA and RRB have been applied to detect Au³⁺ in 50% H₂O in MeCN as a turn-on fluorescent sensor, and the metal interference on Au³⁺ detection is insignificant. Moreover, the fluorescence intensity of rotaxanes is linearly proportional to the concentration of Au³⁺ until excess. RRB can be used for Au³⁺ imaging in HeLa

cells, demonstrating the application of using mechanically interlocked molecules as imaging probes in biological systems.

Conflicts of interest

There are no conflicts to declare.

Acknowledgements

We acknowledge Professor Sir Fraser Stoddart (Department of Chemistry, Northwestern University) for helpful discussions. We thank Dr Xuan Li and Prof. Lijian Jin (Faculty of Dentistry, University of Hong Kong) for the biological studies. We thank Dr Tao Wang (HKBU) for the ESI-MS analysis. This work was partially supported by The State Key Laboratory of Environmental and Biological Analysis as well as The President's Award for Outstanding Performance in Research Supervision to K. C.-F. L. from The Hong Kong Baptist University.

References

- 1 R. M. Duke, E. B. Veale, F. M. Pfeffer, P. E. Kruger and T. Gunnlaugsson, *Chem. Soc. Rev.*, 2010, **39**, 3936.
- 2 X. Zhang, J. Yin and J. Yoon, Chem. Rev., 2014, 114, 4918.
- 3 D. Wu, A. C. Sedgwick, T. Gunnlaugsson, E. U. Akkaya, J. Yoon and T. D. James, *Chem. Soc. Rev.*, 2017, 46, 7105.
- 4 N. De Acha, C. Elosúa, M. J. Corres and J. F. Arregui, *Sensors*, 2019, 19.
- 5 J. F. Stoddart and H. M. Colquhoun, *Tetrahedron*, 2008, **64**, 8231.
- 6 C. J. Bruns and J. F. Stoddart, *The Nature of the Mechanical Bond*, John Wiley & Sons, Inc., Hoboken, NJ, USA, 2016.
- 7 M. J. Langton and P. D. Beer, Acc. Chem. Res., 2014, 47, 1935.
- 8 M. Cirulli, A. Kaur, J. E. M. Lewis, Z. Zhang, J. A. Kitchen, S. M. Goldup and M. M. Roessler, *J. Am. Chem. Soc.*, 2019, 141, 879.
- 9 K. Hiratani, M. Kaneyama, Y. Nagawa, E. Koyama and M. Kanesato, *J. Am. Chem. Soc.*, 2004, **126**, 13568.
- 10 M. Denis, J. Pancholi, K. Jobe, M. Watkinson and S. M. Goldup, *Angew. Chem., Int. Ed.*, 2018, 57, 5310.
- 11 L. M. Hancock, L. C. Gilday, S. Carvalho, P. J. Costa, V. Félix, C. J. Serpell, N. L. Kilah and P. D. Beer, *Chem. Eur. J.*, 2010, **16**, 13082.
- 12 T. Shukla, A. K. Dwivedi, R. Arumugaperumal, C. M. Lin, S. Y. Chen and H. C. Lin, *Dyes Pigm.*, 2016, **131**, 49.
- 13 X. Wang, J. Zhu and D. B. Smithrud, *J. Org. Chem.*, 2010, 75, 3358.
- 14 S.-Y. Hsueh, C.-C. Lai and S.-H. Chiu, *Chem. Eur. J.*, 2010, **16**, 2997.
- 15 W. Zhou, J. Li, X. He, C. Li, J. Lv, Y. Li, S. Wang, H. Liu and D. Zhu, *Chem. – Eur. J.*, 2008, **14**, 754.
- 16 R. Arumugaperumal, V. Srinivasadesikan, M. V. Ramakrishnam Raju, M.-C. Lin, T. Shukla, R. Singh and H.-C. Lin, ACS Appl. Mater. Interfaces, 2015, 7, 26491.

- 17 J. Y. C. Lim, I. Marques, V. Félix and P. D. Beer, *J. Am. Chem. Soc.*, 2017, **139**, 12228.
- 18 J. Y. C. Lim, I. Marques, V. Félix and P. D. Beer, *Angew. Chem., Int. Ed.*, 2018, 57, 584.
- 19 Y.-C. Yeh, B. Creran and V. M. Rotello, *Nanoscale*, 2012, 4, 1871.
- 20 C. F. Shaw, Chem. Rev., 1999, 99, 2589.
- 21 I. Ott, Coord. Chem. Rev., 2009, 253, 1670.
- 22 A. S. K. Hashmi, Chem. Rev., 2007, 107, 3180.
- 23 D. Pflästerer and A. S. K. Hashmi, *Chem. Soc. Rev.*, 2016, 45, 1331.
- 24 R. Ciriminna, E. Falletta, C. Della Pina, J. H. Teles and M. Pagliaro, *Angew. Chem.*, *Int. Ed.*, 2016, 55, 14210–14217.
- 25 A. Habib and M. Tabata, J. Inorg. Biochem., 2004, 98, 1696.
- 26 A. Kundu, R. K. Layek, A. Kuila and A. K. Nandi, *ACS Appl. Mater. Interfaces*, 2012, 4, 5576.
- 27 E. E. Connor, J. Mwamuka, A. Gole, C. J. Murphy and M. D. Wyatt, *Small*, 2005, **1**, 325.
- 28 P. T. Glink, A. I. Oliva, J. F. Stoddart, A. J. P. White and D. J. Williams, *Angew. Chem., Int. Ed.*, 2001, **40**, 1870.
- 29 M. Horn, J. Ihringer, P. T. Glink and J. F. Stoddart, *Chem. Eur. J.*, 2003, **9**, 4046.
- 30 J. Wu, K. C.-F. Leung and J. F. Stoddart, *Proc. Natl. Acad. Sci. U. S. A.*, 2007, **104**, 17266.
- 31 M. E. Belowich, C. Valente and J. F. Stoddart, *Angew. Chem.*, *Int. Ed.*, 2010, **49**, 7208.

- 32 A.-J. Avestro, D. M. Gardner, N. A. Vermeulen, E. A. Wilson, S. T. Schneebeli, A. C. Whalley, M. E. Belowich, R. Carmieli, M. R. Wasielewski and J. F. Stoddart, *Angew. Chem., Int. Ed.*, 2014, 53, 4442.
- 33 Z. Li, X. Han, H. Chen, D. Wu, F. Hu, S. H. Liu and J. Yin, Org. Biomol. Chem., 2015, 13, 7313.
- 34 X. Han, Z. Li, Z. Xu, Z. Zhao, S. H. Liu and J. Yin, *Chin. J. Chem.*, 2017, 35, 1050.
- 35 Z. Li, C. He, Y. Li, Y. Wang, C. Wei, J. Yin and S. H. Liu, *Dyes Pigm.*, 2018, **148**, 130.
- 36 Y.-H. Chang, Y.-J. Lee, C.-C. Lai, Y.-H. Liu, S.-M. Peng and S.-H. Chiu, *Org. Lett.*, 2018, **20**, 2416.
- 37 V. Dvornikovs, B. E. House, M. Kaetzel, J. R. Dedman and D. B. Smithrud, *J. Am. Chem. Soc.*, 2003, **125**, 8290.
- 38 A. Fernandes, A. Viterisi, F. Coutrot, S. Potok, D. A. Leigh, V. Aucagne and S. Papot, *Angew. Chem., Int. Ed.*, 2009, **48**, 6443.
- 39 R. Barat, T. Legigan, I. Tranoy-Opalinski, B. Renoux, E. Péraudeau, J. Clarhaut, P. Poinot, A. E. Fernandes, V. Aucagne, D. A. Leigh and S. Papot, *Chem. Sci.*, 2015, 6, 2608.
- 40 G. Yu, D. Wu, Y. Li, Z. Zhang, L. Shao, J. Zhou, Q. Hu, G. Tang and F. Huang, *Chem. Sci.*, 2016, 7, 3017.
- 41 W.-Y. Wong, K. C.-F. Leung and J. F. Stoddart, *Org. Biomol. Chem.*, 2010, **8**, 2332.
- 42 M. Baruah, W. Qin, C. Flors, J. Hofkens, R. A. L. Vallée, D. Beljonne, M. Van der Auweraer, W. M. De Borggraeve and N. Boens, J. Phys. Chem. A, 2006, 110, 5998.